Superlattices and Microstructures 75 (2014) 378–389

Contents lists available at ScienceDirect

Superlattices and Microstructures

journal homepage: www.elsevier.com/locate/superlattices

Structural and optical characterization of ZnO thin films for optoelectronic device applications by RF sputtering technique

Shashikant Sharma [a], Sumit Vyas [c], C. Periasamy [a,b,*], P. Chakrabarti [c,d]

[a] Department of Electronics and Communication Engineering, Malaviya National Institute of Technology, Jaipur, Rajasthan 302017, India
[b] Material Research Centre, Malaviya National Institute of Technology, Jaipur, Rajasthan 302017, India
[c] Centre of Interdisciplinary Research, Motilal Nehru National Institute of Technology, Allahabad 211004, U.P., India
[d] Department of Electronics Engineering, Indian Institute of Technology (IIT-BHU), Varanasi 221005, India

ARTICLE INFO

Article history:
Received 9 July 2014
Received in revised form 20 July 2014
Accepted 22 July 2014
Available online 9 August 2014

Keywords:
Thin films
RF sputtering
Structural properties
Surface properties
Optical properties

ABSTRACT

This work reports structural and optical study of ZnO thin films grown over p-type silicon (Si) and glass substrates by RF magnetron sputtering technique. Surface morphological and optical properties of thin film have been studied using X-ray Diffraction (XRD), Atomic Force Microscopy (AFM), Scanning Electron Microscopy (SEM), Energy-Dispersive X-ray (EDX), ellipsometry and photoluminescence (PL) spectroscopy. Strong diffraction peak (002) obtained from XRD spectra of ZnO thin film indicates a preferential growth of single crystalline thin film along the *c*-axis oriented phase of hexagonal wurtzite structure. Surface morphological feature reveals uniform growth of undoped ZnO thin film over the substrate. Different important microstructural parameters for the film such as grain size, lattice parameters, defect density, stress and strain have been obtained. Optical properties such as transmittance, reflectance, absorption coefficient, refractive index and dielectric constant for a spectral range of 300–800 nm have been evaluated. A good optical transmittance of 83–92% has been observed for visible region, and the optical bandgap of ZnO films

* Corresponding author at: Department of Electronics and Communication Engineering, Malaviya National Institute of Technology, Jaipur, Rajasthan 302017, India. Tel.: +91 1412713232 (O); fax: +91 01412529029.
E-mail address: cpsamy.ece@mnit.ac.in (C. Periasamy).

http://dx.doi.org/10.1016/j.spmi.2014.07.032

was found to be 3.23 eV. Energy Loss Function (ELF) and photoluminescence (PL) spectra for ZnO thin film has also been analyzed and reported.

1. Introduction

In recent years, ZnO has emerged as a promising material for a variety of optoelectronic and piezoelectric device applications. Its large bandgap (3.37 eV) and high exciton binding energy (60 meV) ensures its suitability for a variety of applications such as photodetectors (UV), room temperature LEDs, solar cells and gas sensors [1–4]. High exciton binding energy of ZnO attributes to stability of electron–hole pairs at room temperature for electroluminescence. Therefore, ZnO is a potential candidate for highly efficient lasers and LEDs, provided a good quality of p-doped ZnO thin film can be grown. Good and stable photoluminance of ZnO at higher temperature ranges makes it an extremely promising material for variety of optoelectronic device applications [5]. ZnO's blue region electromagnetic spectrum emission capability, high light–matter coupling strength and stability of its excitons at room temperature is very useful for the realization of new generation optoelectronic devices such as polariton lasers at room temperature [6]. High piezoelectric coefficient and large electromechanical coupling coefficient of ZnO nanostructures ensure its usability for piezoelectric and micro-electromechanical (MEMS) device applications [7–9].

ZnO nanostructures with single crystalline orientation along the *c*-axis are important for improved device performance in a variety of nanoelectronic applications. In the past, different techniques such as sol–gel, thermal vapor deposition, pulsed laser deposition, e-beam deposition and RF sputtering have been reported for growing ZnO thin films [10–13]. Among these methods, RF sputtering has drawn wide attention. In RF sputtering, different parameters such as pressure, temperature, deposition time, gas flow rate and RF power can control the properties of grown thin films. Easy control for desired crystalline orientation, good interfacial adhesion with substrate, epitaxial growth at relatively low temperature and high packing density of grown thin film are some properties which make RF sputtering a suitable choice for growing ZnO thin films. This work reports a systematic study of structural and optical properties of ZnO thin film deposited on p-type Si and glass substrates using RF sputtering technique. Different microstructural (crystallographic orientation, roughness, grain size, lattice parameters, defect density, stress, strain) and optical parameters (transmittance, reflectance, optical bandgap, refractive index, dielectric constant, surface and volume energy loss function, photoluminescence) of the deposited ZnO thin film have been studied and reported.

2. Experimental details

2.1. ZnO thin film preparation

Nanocrystalline ZnO thin film was deposited on p-Si ⟨1 0 0⟩ and glass substrate using RF magnetron sputtering technique. Thickness and resistivity of p-Si substrate was 380 μm and 8–10 Ω cm respectively. Prior to deposition, both Si wafer and glass substrate were cleaned properly. Standard RCA-1 and RCA-2 cleaning process were used for wafer cleaning. RCA-1 (Solution of NH_4OH, H_2O_2 and Deionized Water (DI) in the ratio of 1:1:5) was used for removal of organic contamination and RCA-2 (Solution of HCl, H_2O_2 and DI water in the ratio of 1:1:6) was used for removal of ionic contamination from the Si wafer. Glass substrate was cleaned with acetone and isopropanol, and then rinsed in deionized water before fixing it to the substrate holder. ZnO thin film was deposited over Si and glass substrate at room temperature using ZnO target (3-inch dia target) made up of 99.9% pure ZnO powder from MERK Chemical Limited, Mumbai, India. RF & DC magnetron sputtering system from Advanced Process Technologies, India was used for depositing ZnO thin film. Base pressure, deposition pressure and

deposition time were set as 5×10^{-6} mbar, 3×10^{-3} mbar and 30 min respectively. Deposition rate was varied from 0.7 Å/s to 1.7 Å/s while argon flow rate was maintained at 22 sccm during the deposition. Deposited film was subsequently annealed for 30 min at 400 °C in argon ambient. After annealing samples were cooled to reach room temperature before studying structural, morphological and optical properties of ZnO thin film samples.

2.2. Thin film characterization

The crystal structure and morphology of the sample were characterized with the help of X-ray Diffractometer (PANalytical X'Pert Pro), Atomic Force Microscope (Multimode-8 Scanning Probe Microscope from Bruker) and Scanning Electron Microscope (Nova Nano FE-SEM 450 Model). Thickness measurement and optical characterization of ZnO thin film have been done using ellipsometer (Model: VWASE VB-400 from J.A. Woollam Co.). The photoluminescence spectra of ZnO thin film was studied by photoluminescence (PL) spectroscope (Perkin Elmer, USA) using 325 nm wavelength of a He–Cd laser at room temperature.

3. Results and discussion

3.1. Structural and surface morphology study

Fig. 1 shows XRD spectra of ZnO thin film. A unique diffraction peak corresponding to 002 orientation at $2\theta = 34.48°$ was obtained. This confirms single crystalline nature of the deposited ZnO thin film. The unique peak obtained from XRD results also attributes to good crystallinity of ZnO thin film along the *c*-axis. Various important micro-structural parameters such as grain size, lattice parameters, defect density, residual stress and lattice strain for ZnO thin film have also been derived. Grain size of 22 nm for (002) crystallographic plane have been obtained using Scherrer's formula [14].

$$D = \frac{0.94\lambda}{\beta \cos\theta} \tag{1}$$

where λ is X-ray wavelength, β is full-width-half-maximum (FWHM) of the diffraction peak and θ is the diffraction angle. Lattice Parameters (a, b, c) have been calculate using Eqs. (2) and (3). The values for $a = b$, c were found to be 3.013 Å and 5.21 Å respectively. These parameters shows a good agreement with standard JCPDS data (PDF #36-1451 ($a = b = 3.25$ Å, $c = 5.20$ Å)) for lattice parameters [14].

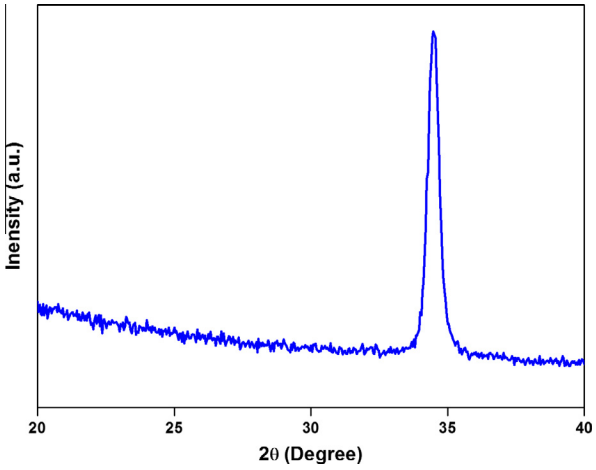

Fig. 1. XRD spectra of ZnO thin film.

$$a = b = \frac{\lambda}{\sqrt{3}\sin\theta} \tag{2}$$

$$c = \frac{\lambda}{\sin\theta} \tag{3}$$

Dislocation density which can be described as length of dislocations per unit volume is useful to obtain information about crystal structure of grown thin film and can be calculated as [15]:

$$\text{Dislocation Density} = \frac{1}{D^2} \tag{4}$$

The value obtained for dislocation density from Eq. (4) is 2.06×10^{-3} nm^{-2}. Smaller value of dislocation density attributes to better crystallization of the thin film. Lattice strain and residual stress have been obtained using Eqs. (5) and (6):

$$\text{Lattice Strain} = \frac{\beta}{4\tan\theta} \tag{5}$$

$$\text{Residual Stress } (\sigma) = -233\frac{(c - c_0)}{c_0}\,[\text{Gpa}] \tag{6}$$

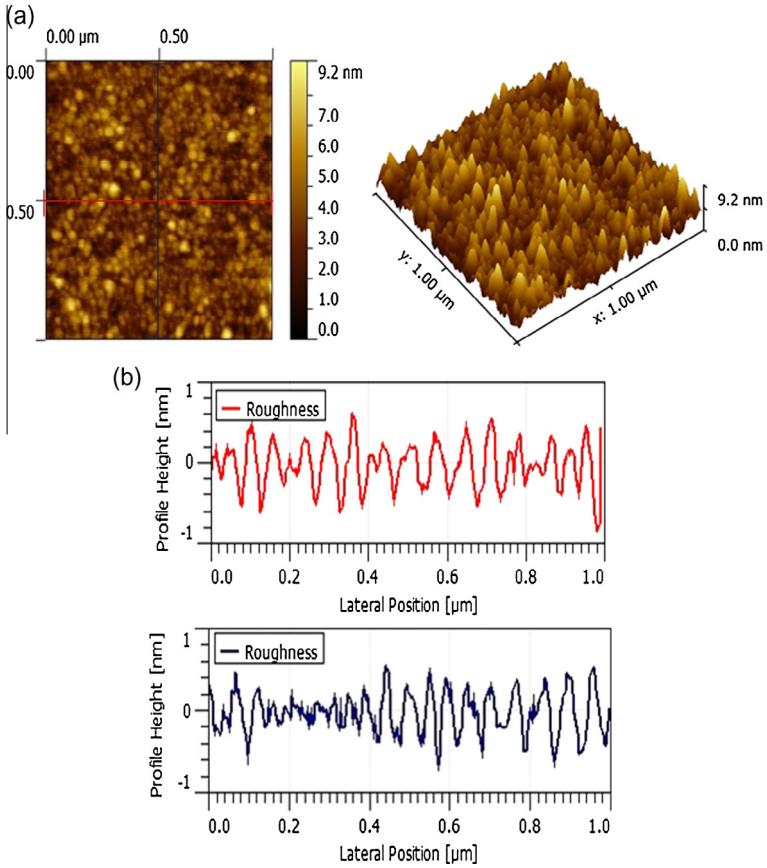

Fig. 2. (a) Two and three-dimensional AFM images of ZnO thin film on Si substrate and (b) roughness profile plot of ZnO thin film for scanning area highlighted in Fig. 2(a).

where c_0 (5.206 Å) is the unstrained lattice constant for bulk ZnO [16,17]. Values obtained for residual stress and strain are -0.537 GPa and 5.56×10^{-3} respectively. Negative sign obtained for residual stress signifies that the stress for the prepared thin film is compressive. The atomic force microscope (AFM) image (Fig. 2(a)) clearly demonstrates that, good surface morphology for ZnO thin film can be grown on p-Si substrate using RF sputtering technique. Fig. 2(b) demonstrates roughness profile of the grown film for a scanning area of 1 μm × 1 μm. The root mean square roughness obtained from horizontal and vertical scanning highlighted in Fig. 2(b) were 0.255 nm and 0.248 nm respectively. This feature of ZnO thin film ensures its suitability for nanoelectronic device applications. Fig. 3(a) shows scanning electron microscope (SEM) image of ZnO thin film at 100k×, magnification. It has been observed that surface morphology of grown ZnO film is almost uniform and homogeneous. It can be noticed from SEM image that film is composed of regular round grains with grain size varying in the range of 20–40 nm. Fig. 3(b) depicts Energy-Dispersive X-ray (EDX) spectrum of ZnO thin film annealed at 400 °C for 30 min. EDX spectra confirmed the presence of zinc and oxygen content in the deposited film. The silicon peak appears due to substrate. The inset in Fig. 3(b) shows the corresponding weight percent of the elements present in the film and result obtained further assures that no other impurity is present in the film.

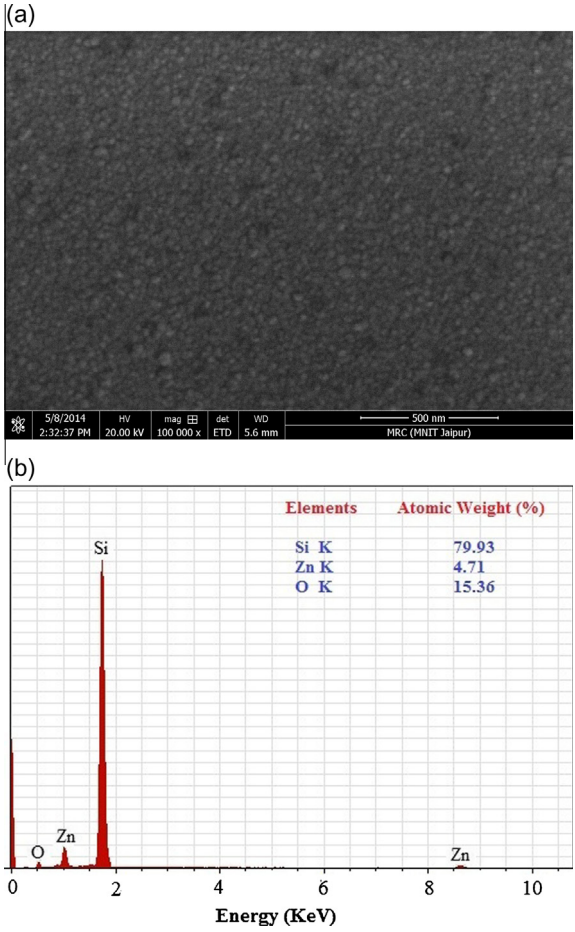

Fig. 3. (a) SEM image of ZnO thin film and (b) EDX spectra for ZnO/Si heterojunction (inset shows elements present by their corresponding atomic weight %).

3.2. Optical properties

Figs. 4 and 5 show transmittance and reflectance spectra of ZnO thin film in 300–800 nm wavelength range. A strong transmittance of 83–92% has been observed for visible region which ensures its suitability for use as transparent window material in a variety of optoelectronic device applications. Reflectance spectra shown in Fig. 5 depicts low optical reflection of 10–18% for the wavelength range of 300–800 nm. It has been observed that as the wavelength increases in visible region, reflectivity decreases. The reflection peak near the bandgap wavelength attributes to interband transition from valance band to conduction band. Low reflectance of ZnO thin film makes it a suitable choice for anti-reflecting coating materials. The absorption coefficient (α) for ZnO thin film (shown in Fig. 6) has been calculated using Beer–Lambert's law [18]:

$$\alpha = \frac{1}{d}\ln\frac{1}{T} = \frac{2.303}{d}A \tag{7}$$

where d is ZnO film thickness (95 nm in our case as measured from ellipsometric measurement) and T is the transmittance of thin film. The absorption spectra shown in the inset of Fig. 6 can be divided into two regions. It can be seen from the graph that a strong absorbance has been observed for shorter wavelengths ($\lambda < 370$ nm) and a low absorbance has been observed for longer wavelengths ($\lambda > 370$ nm). Photons having energy equal to or higher than the bandgap of ZnO provides sufficient energy for excitation of electrons from valance band to conduction band which is the probable reason for strong absorbance in shorter wavelength ranges. Interstitial Zn and oxygen are responsible for conductivity of ZnO film. Since low energy of incident light is sufficient enough to ionize these impurities, ZnO has shown low absorbance for larger wavelengths. It has also been observed that transmittance and absorbance spectra for a typical thin film has shown inverse relationship which signifies that ZnO behaves as opaque material for shorter wavelengths ($\lambda < 370$ nm) and behaves as transparent material at longer wavelengths ($\lambda > 370$ nm). In addition, relation between incident photon energy ($h\nu$) and absorption coefficient (Eq. (8)) have been used to obtain optical bandgap of ZnO thin film [19].

$$\alpha h\nu = B(h\nu - E_g)^n \tag{8}$$

where α is absorption coefficient, $h\nu$ is photon energy, E_g is optical bandgap and B is constant depending upon the probability of absorption and refractive index of the material. Since ZnO material has direct transition mechanism, value of n is taken as 1/2. Fig. 7 shows $(\alpha h\nu)^2$ versus incident photon energy ($h\nu$) plot for ZnO thin film. The energy bandgap of deposited thin film can be estimated from

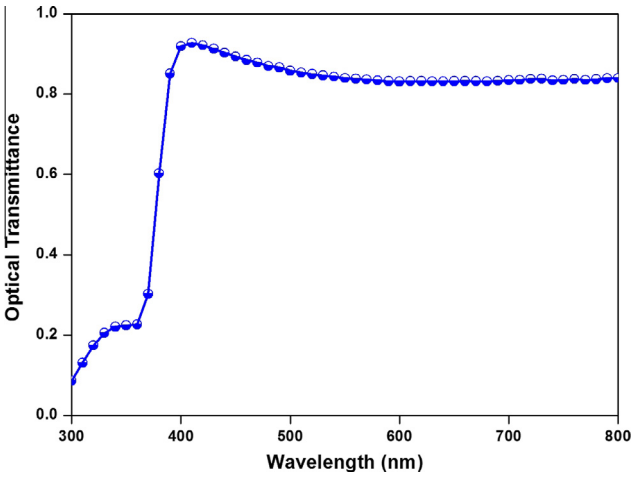

Fig. 4. Optical transmittance spectra obtained for ZnO thin film.

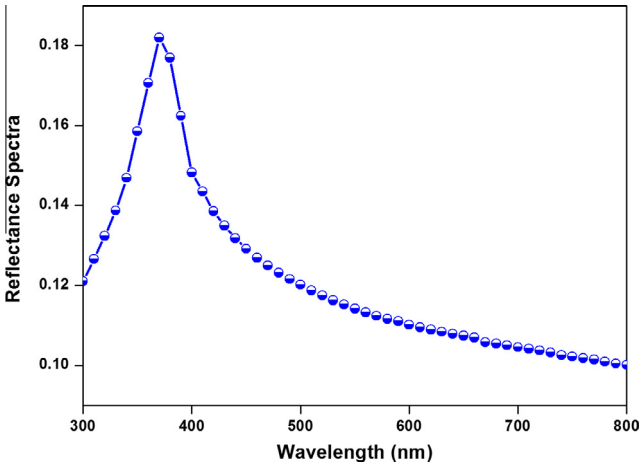

Fig. 5. Optical reflectance spectra obtained for ZnO thin film.

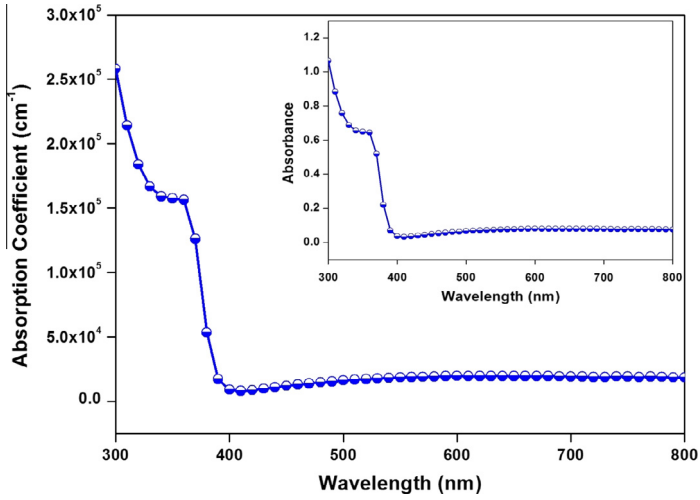

Fig. 6. Absorption coefficient spectra obtained for ZnO thin film (inset shows absorbance spectra of ZnO thin film).

the extrapolation of the linear portion of $(\alpha h\nu)^2$ versus $(h\nu)$ plot over $h\nu$ axis. The value of energy band-gap was estimated to be 3.23 eV for ZnO thin film. The variation of absorption coefficient with photon energy for ZnO film is demonstrated in Fig. 8. Urbach relation which governs such dependence can be written as [20,21]:

$$\alpha = \alpha_0 \exp\left(\frac{E}{E_u}\right) \tag{9}$$

where E is photon energy, E_u is Urbach energy and α_0 is band tailing parameter which can be obtained as:

$$\alpha_0 = \sqrt{\frac{\sigma_0\left(\frac{4\pi}{c}\right)}{n\Delta E}} \tag{10}$$

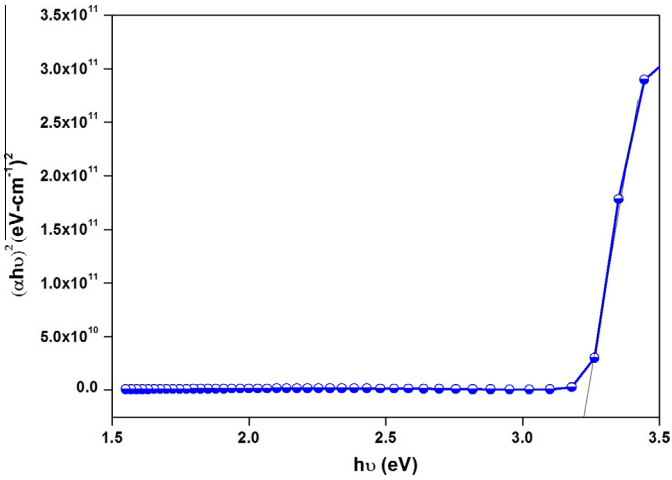

Fig. 7. $(ahv)^2$ versus (hv) plot for bandgap evaluation in deposited ZnO thin film.

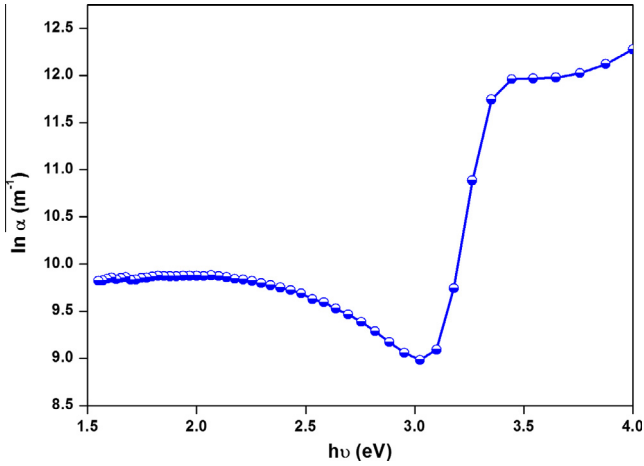

Fig. 8. ln(α) versus photon energy plot for ZnO thin film.

where σ_0 is electrical conductivity at absolute zero, c is velocity of light, ΔE is the width of the tail of localized states in the forbidden gap. Urbach energy has been obtained from Fig. 8 by taking the reciprocal of the slope in linear region. The value obtained for Urbach energy is 85 meV which is in good agreement with that reported by Gadallah et al. [21]. Refractive index is a key parameter for optical materials deployed in integrated optic devices such as modulators, switches, and filters. It is closely related to local field and electronic polarization of ions in the material. The refractive index can be obtained using following equation [22].

$$n = \sqrt{\frac{4R}{(1-R)^2} - k^2} + \left(\frac{1+R}{1-R}\right) \tag{11}$$

where the extinction coefficient, k is given by:

$$k = \frac{\alpha\lambda}{4\pi} \tag{12}$$

α is the absorption coefficient and R is reflectivity of thin film. Refractive index versus wavelength plot and extinction coefficient versus wavelength plot (inset Fig. 9) obtained from ellipsometry measurement is shown in Fig. 9. It can be seen from Fig. 9 that the refractive index of the film first increases with increase in wavelength, attains a maximum value at ~370 nm wavelength and then decreases with further increase in wavelength. The dielectric constant of ZnO thin film can be expressed as [23]:

$$\epsilon(\omega) = \epsilon_{\text{real}}(\omega) + \epsilon_{\text{img.}}(\omega) \tag{13}$$

where the real and imaginary parts of dielectric constant can be expressed as:

$$\epsilon_{real} = n^2 - k^2 \tag{14}$$

$$\epsilon_{img.} = nk \tag{15}$$

Figs. 10 and 11 show the real and imaginary parts of the dielectric constant plot for ZnO thin film. The peak observed near the ZnO bandgap wavelength is attributed to strong interaction between electrons and photons at this wavelength. The real and imaginary parts of the dielectric constant exhibit the variations in the range of 3.7–6.1 and 0–1.8 respectively for a wavelength range of 300–800 nm. The study of energy loss function of metal oxides is also important to ensure the suitability of the material for optical communication applications. Thus, volume and surface energy loss functions (Eqs. (16) and (17)) for ZnO thin film have been evaluated to understand the energy loss of the fast moving electrons traveling in the bulk and surface of the films [24,25].

$$\text{VELF} = \frac{\varepsilon_{\text{img.}}}{\epsilon^2_{\text{real}} + \epsilon^2_{\text{img.}}} \tag{16}$$

$$\text{SELF} = \frac{\varepsilon_{\text{img.}}}{(\varepsilon_{\text{real}} + 1)^2 + \epsilon^2_{\text{img.}}} \tag{17}$$

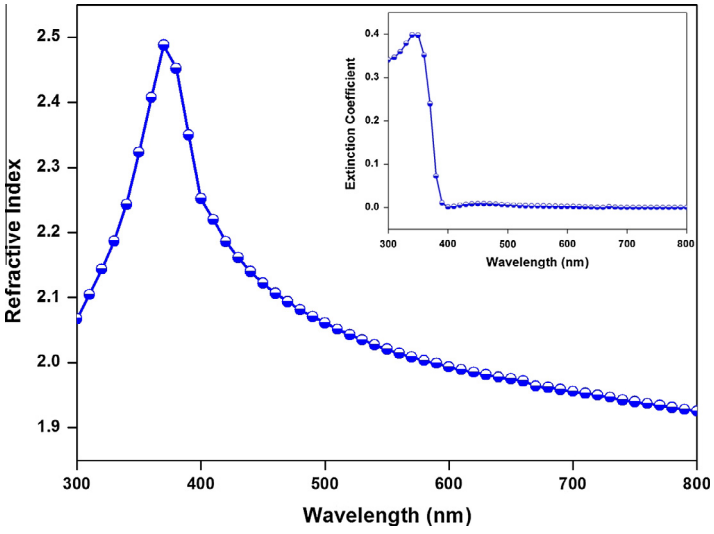

Fig. 9. Refractive index versus wavelength graph for ZnO thin film (inset shows extinction coefficient versus wavelength plot).

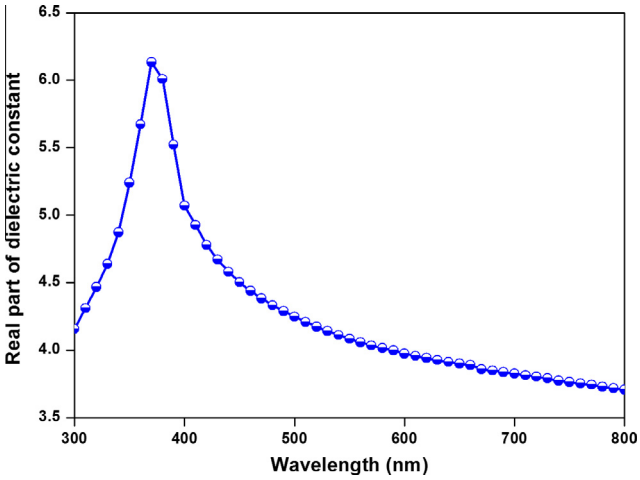

Fig. 10. Real part of dielectric constant versus wavelength for ZnO thin film.

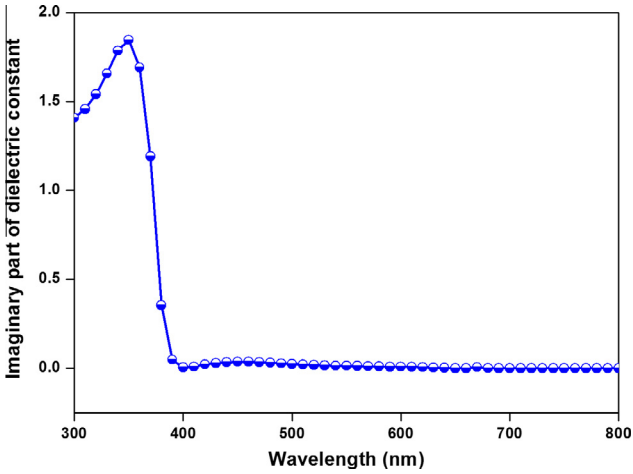

Fig. 11. Imaginary part of dielectric constant versus wavelength plot.

Fig. 12 shows the variation of Volume Energy Loss Function (VELF) and Surface Energy Loss Function (SELF) with photon energy. It is observed from Fig. 12 that both volume and surface energy loss functions have high value at higher photon energy. It has also been observed that the qualitative behavior of VELF, SELF variations is similar and value of VELF is higher than SELF for photon energy beyond 3.2 eV.

Fig. 13 illustrates photoluminescence (PL) spectra of ZnO thin film grown over p-Si (1 0 0) substrate. PL spectra has shown a sharp UV peak centered at 377 nm which indicates that a good quality ZnO thin film has been grown over Si substrate. Careful analysis reveals that two more peaks (centered at 433 nm and 572 nm) with very low intensity as compared to UV peak also exist in the PL spectra. The first peak (377 nm, UV emission) attributes to excitonic emission, band to band transition and donor–acceptor pair transitions. Violet emission centred at 433 nm may be attributed to radiative defects related to interface traps existing at grain boundaries leading to radiative transition between this level and the valence band [26]. Wang et al. suggested that the transition of electrons from

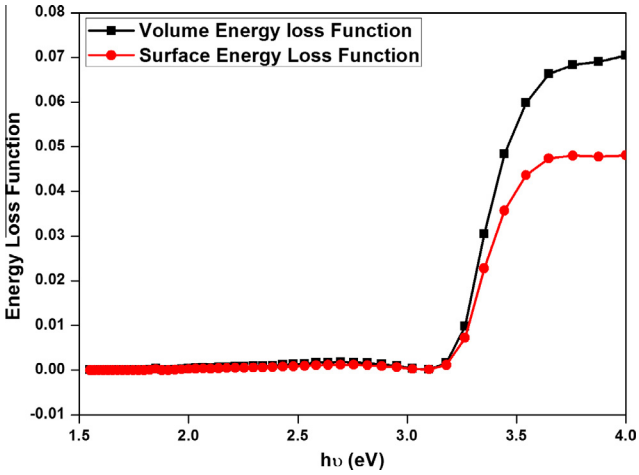

Fig. 12. Energy loss function versus photon energy plot for ZnO thin film.

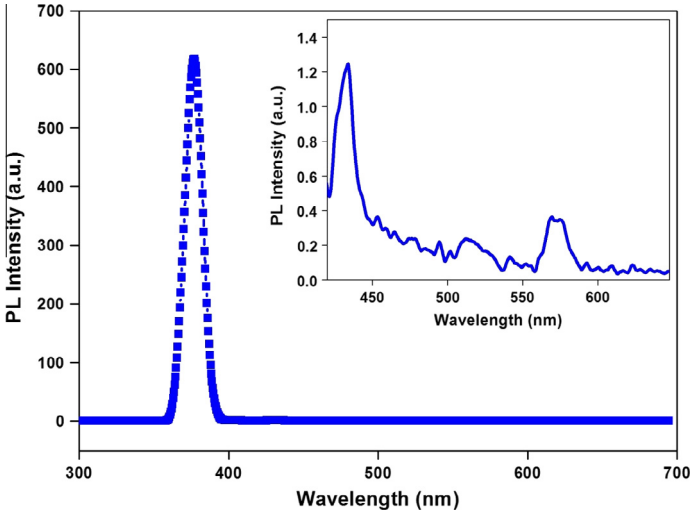

Fig. 13. PL spectra of deposited ZnO thin film.

conduction band tail to valance band tail could be the probable reason for this violet emission [27]. Green–yellow emission (centred at 572 nm) is understood to be caused by deep level emission which attributes to oxygen vacancies, zinc vacancies or zinc interstitials [28].

4. Conclusion

Preparation of nanocrystalline ZnO thin film grown by RF sputtering technique has been reported. It has been observed that RF sputtered ZnO thin film has shown a good crystalline nature with minimal surface roughness. Different microstructural parameters of thin film have been estimated using XRD analysis. A very good transmittance of 83–92% has been observed in the visible region for ZnO thin film. Optical band gap was found to be 3.23 eV. Various other optical parameters such as

reflectance, absorbance, refractive index, dielectric constant, energy loss function and PL spectra have also been analyzed and reported. Results confirm that a high quality ZnO thin film can be grown using RF magnetron sputtering technique for potential use in a variety of optoelectronic devices.

Acknowledgement

The authors are thankful to Material Research Centre, Malaviya National Institute of Technology, Jaipur, Rajasthan, India and Centre of Interdisciplinary Research, Motilal Nehru National Institute of Technology, Allahabad, U.P., India for extending fabrication and characterization related facilities to complete this work.

References

[1] R. Romero, M.C. Lopez, D. Leinen, F. Martin, J.R. Ramos-Barrado, Mater. Sci. Eng.: B 110 (2004) 87–93.
[2] R. Ghosh, D. Basak, Appl. Phys. Lett. 90 (2007). 243106-3.
[3] S. Sharma, C. Periasamy, Superlattices Microstruct. 73 (2014) 12–21.
[4] S. Sharma, C. Periasamy, J. Electron Dev. 19 (2014) 1633–1636.
[5] L. Beaur, T. Bretagnon, B. Gil, A. Kavokin, T. Guillet, C. Brimont, D. Tainoff, M. Teisseire, J.-M. Chauveau, Phys. Rev. B 84 (2011) 165312–165318.
[6] M. Zamfirescu, A. Kavokin, B. Gil, G. Malpuech, M. Kaliteevski, Phys. Rev. B 65 (2002). 161205-4.
[7] Z.L. Wang, J. Song, Science 312 (2006) 242–246.
[8] J.L. Deschanvres, P. Rey, G. Delabouglise, M. Labeau, J.C. Joubert, Sens. Actuators A 33 (1992) 43–45.
[9] R. Singh, M. Kumar, S. Chandra, J. Mater. Sci. 42 (2007) 4675–4683.
[10] L. Znaidi, Mater. Sci. Eng. B 174 (2010) 18–30.
[11] B.D. Yao, Y.F. Chan, N. Wang, Appl. Phys. Lett. 81 (2002). 757-3.
[12] S.H. Bae, S.Y. Lee, B.J. Jin, S. Im, Appl. Surf. Sci. 169–170 (2001) 525–528.
[13] R. Al Asmar, D. Zaouk, Ph. Bahouth, J. Podleki, A. Foucaran, Microelectron. Eng. 83 (2006) 393–398.
[14] B.D. Cullity, S. Rstock, Elements of X-Ray Diffraction, Prentice Hall, New Jersey, NJ, USA, 2001.
[15] V. Bilgin, S. Kose, F. Atay, I. Akyuz, Mater. Chem. Phys. 94 (2005) 103–108.
[16] H.P. Klug, L.E. Alexander, X-Ray Diffraction Procedures for Polycrystalline and Amorphous Materials, Wiley, New York, NY, USA, 1974.
[17] Y.G. Wang, S.P. Lau, H.W. Lee, S.F. Yu, B.K. Tay, X.H. Zhang, K.Y. Tse, H.H. Hng, J. Appl. Phys. 94 (2003) 1597–1604.
[18] S. Aydogu, O. Sendil, M.B. Coban, Chinese J. Phys. 50 (2012) 89–100.
[19] J. Tauc, Amorphous and Liquid Semiconductors, Plenum, London, UK, 1974.
[20] F. Urbach, Phys. Rev. 92 (1953) 1324.
[21] A.S. Gadallah, M.M. El-Nahass, Adv. Condens. Mat. Phys. 2013 (2013) 1–11.
[22] M. Di Giulio, G. Micci, R. Rella, P. Siciliano, A. Tepore, Phys. Status Solidi A 136 (1993) K101–K104.
[23] T.S. Moss, G.J. Burrell, B. Ellis, Semiconductor Opto-Electronics, Wiley, New York, 1973.
[24] R.K. Gupta, M. Cavas, F. Yakuphanoglu, Spectrochim. Acta Part A Mol. Biomol. Spectrosc. 95 (2012) 107–113.
[25] A.M. Salem, T.M. Dahy, Y.A. El-Gendy, Physica B: Phys. Condens. Mat. 403 (2008) 3027–3033.
[26] B.J. Jin, S. Im, S.Y. Lee, Thin Solid Films 366 (2000) 107–110.
[27] Q.P. Wang, D.H. Zhang, Z.Y. Xue, X.T. Hao, Appl. Surf. Sci. 201 (2002) 123–128.
[28] F.H. Leiter, H.R. Alves, A. Hofstaetter, D.M. Hofmann, B.K. Meyer, Phys. Status Solidi B 226 (2001) R4–R5.